A Thesis to opt to the degree of MSc in Automatic Control

Estimation of Average Power Consumption of Electric Vehicles based on Inaccurate Positioning Data

Javier A. Torres B.

June 23, 2025

Universidad Técnica Federico Santa María
Electronics Department

CONSTANCIA DE VALIDACIÓN Y CONFIDENCIALIDAD DE MONOGRAFÍA A REPOSITORIO ACADÉMICO

1.- IDENTIFICACIÓN DEL TRABAJO ACADÉMICO

Tipo de monografía (marcar una opción): ☐ Memoria o trabajo de título; ☒ Tesis de Postgrado;

Título del trabajo: Estimation of Average Power Consumption on Electric Vehicles based on Inaccurate Positioning Data

Nombre del candidato(a): Javier Alejandro Torres Bustos

Carrera / Grado: Magíster en Ciencias de la Ingeniería Electrónica

Campus: Casa Central Valparaiso**;** **Departamento**: Departamento de Electrónica

2.- VALIDACIÓN DEL PROFESOR GUÍA/DIRECTOR DE TESIS

Yo, César Silva Jiménez, en mi calidad de profesor(a) guía/director(a) del trabajo académico mencionado anteriormente **DEJO CONSTANCIA** que:

- He revisado esta versión del documento y corresponde a la versión final aprobada del trabajo.
- El trabajo cumple con los requisitos académicos y de formato establecidos por la institución

3.- EVALUACIÓN DE CONFIDENCIALIDAD POR PROPIEDAD INDUSTRIAL

☒ El trabajo **NO contiene información que amerite confidencialidad** y puede ser publicado de inmediato en repositorio con acceso abierto.

☐ El trabajo **CONTIENE** información con potenciales implicancias de propiedad industrial o intelectual y requiere un periodo de confidencialidad (embargo) por:

☐ 6 meses; ☐ 12 meses; ☐ 2 años; ☐ 3 años; ☐ 5 años; ☐ 10 años

Fundamentación de la necesidad de confidencialidad (obligatorio si se solicita embargo):

4.- FIRMAS

Profesor(a) guía o director(a) de memoria o tesis:

Fecha: 23/06/2025 ; **Firma:** _____

Estudiante o Candidato(a):

Fecha: 23/06/2025 ; **Firma:** _____

Este formulario debe ser insertado como página 2 de la memoria o tesis, completado y firmado por estudiante y profesor(a) antes de la entrega en portal PRISMA de Biblioteca USM.

Abstract

The urgent need to decrease the global carbon footprint is pushing industries such as mining, transportation, and agriculture to replace internal combustion engines (ICE) in their vehicles with electrically powered ones. However, the range of electric vehicles (EVs) remains significantly lower than their ICE counterparts. Thus, it is of paramount importance to deliver accurate estimates of power consumption (and remaining range) for energy-efficient route planning applications.

In this thesis, a method is proposed for estimating Instantaneous Power Consumption (IPC) of an EV from inaccurate positioning data, with the goal of obtaining an accurate estimate of average power consumption over a given path. The performance of the proposed method is experimentally validated on different terrains and sources of positioning data. Average power consumption derived from electrical monitoring (via onboard voltage and current sensors) is used to determine experimental performance in terms of its accuracy.

Resumen

La urgente necesidad de reducir la huella de carbono global está impulsando a industrias como la minería, el transporte y la agricultura a reemplazar los motores de combustión interna en sus vehículos por motores eléctricos. Sin embargo, la autonomía de los vehículos eléctricos sigue siendo significativamente inferior a la de sus contrapartes de combustión interna. Por lo tanto, es de suma importancia obtener estimaciones precisas del consumo de potencia (y de la autonomía restante) para aplicaciones de planificación de rutas energéticamente eficientes.

En esta tesis, se propone un método para estimar el Consumo Instantáneo de Potencia de un vehículo eléctrico a partir de datos de posicionamiento inexactos, con el objetivo de obtener una estimación precisa del consumo promedio de potencia a lo largo de una ruta determinada. El desempeño del método propuesto se valida experimentalmente con diferentes terrenos y fuentes de datos de posicionamiento. El consumo promedio de potencia derivado a partir del monitoreo eléctrico (mediante sensores de voltaje y corriente a bordo) se utiliza para determinar el desempeño experimental en términos de su precisión.

Contents

List of Figures

List of Tables

1. Introduction

1.1. Context

The urgent need to decrease the global carbon footprint, coupled with great public attention, is pushing industries such as mining, transportation and agriculture to seek more sustainable operations. In this effort, there is an ongoing transition towards the use of electrically powered machinery, fueled by green energy. In particular, electric vehicles (EVs) are gradually replacing internal combustion engine (ICE) vehicles.

However, the range of EVs remains significantly lower than their ICE counterparts [1, 2], and the available infrastructure for fossil fuel supply greatly exceeds that of charging stations for EVs [3–5]. This results in limited EV adoption and a slow transition to electromobility.

There are two main approaches to the EV range problem:

1. Improving battery technology in terms of a higher energy density and enhanced charging cycles [5, 6].
2. Developing better, energy-efficient, route planning solutions [7–9].

The first approach has a great impact in the private transportation industry, where expected power consumption is unknown and mainly depends on user's driving patterns and traffic conditions [10, 11]. The second approach is of great importance in the mining and agriculture industry, where routes and loads can be planned ahead and optimized, taking range limitations into account. The focus of this thesis falls into the latter category.

1.2. Related work

The energy consumption of vehicles (whether based on combustion engines or electric ones) has been a topic of research for the past few decades. A key variable in this context is Instantaneous Power Consumption (IPC)[12], as its average value is directly related to energy consumption and therefore remaining range.

In urban transportation applications, a highly unstructured scenario, power consumption is intrinsically related to the human behaviour behind the wheel [10, 13, 14] (that is -of course- in non-autonomous vehicles, still the most common case for urban transportation). In consequence, there is increasing interest in modelling human driving styles, their relation to traffic and how they impact IPC, as discussed in [14–16] (and the references therein). As the transition to electromobility progresses, the need for informed planning of the location of EV charging stations [4, 5, 17] has driven the attention of the scientific community to the creation of urban power consumption maps [14, 15]. Such maps are geo-positioned information of the power consumption of different electric vehicles and are usually devoted to cities, as shown in [18, 19].

In other industries, such as agriculture or mining, energy consumption is typically not affected by traffic conditions, and there exists a specific route to be followed by the vehicle or fleet [6, 20]. This more structured scenario allows for more accurate estimation and prognosis of the IPC of a vehicle. This information has great potential benefits through energy-efficient route planning, such as optimizing battery usage, planning when and where to charge batteries, evaluating the feasibility of following a given route and determining the amount of machinery to use, among others [12].

A commonly considered method for IPC estimation is to measure voltage and current across battery terminals, and compute their product [2, 3, 12, 21]. However, these measurements are often not available or have limited resolution, and yield a power estimate with poor statistical performance [22]. As an alternative, an analytical model has been successfully employed by several authors [2, 3] to estimate EV's power consumption considering multiple vehicle and terrain parameters. This model explains how electric power is converted into tractive power, considering the effect of wheel-terrain interactions, fluid resistance and motor dynamics. This model is presented in detail in Chapter 2.

A key to successfull estimation of IPC by means of this analytical model is the adoption of a stochastic framework [23–26]. Thus, attempts as the ones shown in [27, 28] where a deterministic framework was used showed non-concluding results. In this thesis, a stochastic framework is adopted.

It should be noted that, despite the success of the analytical model under a stochastic framework in the literature, there are relevant variables being left unaccounted for. For instance, researchers have shown that temperature, both inside and outside the engine and batteries, has a great impact on IPC [3, 12, 22].

1.3. Proposal

In this thesis, a method is developed to yield estimates of average power consumption from inaccurate vehicle positioning data. This method provides a simple, robust and widely available alternative for estimating the average power consumption of EV's, as positioning systems are commonly equipped on EVs in the form of a Global Navigation Satellite System (GNSS).

The proposed method expands on the analytical model mentioned in the previous section. This model is a function of the vehicle's velocity and acceleration, and a set of vehicle and terrain parameters identified beforehand. However, non-accelerated linear motion is assumed. Thus acceleration is disregarded and only velocity needs to be estimated from vehicle positioning. An optimal velocity estimate is obtained in terms of minimal bias and variance of the resulting IPC estimate. The general architecture of the proposed method is depicted in Figure 1.1.

The performance of the proposed method is experimentally validated on different terrains and sources of positioning data. Average power consumption derived from electrical monitoring (via onboard voltage

and current sensors) is used to determine experimental performance in terms of its accuracy.

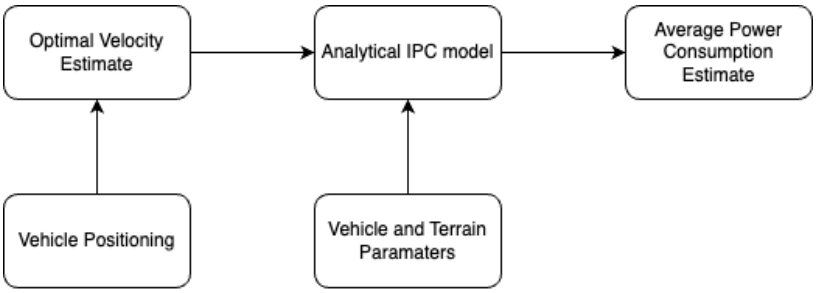

Figure 1.1.: General overview of the proposed average power consumption estimation method.

1.4. Organization

This Thesis is organized as follows: Chapter 2 shows the problem statement in detail, presenting the mathematical notation to be used and the analytical model for IPC that will serve as basis for the proposed method. Chapter 3 presents a detailed explanation of the proposed IPC estimation method using vehicle localization data. Chapter 4 shows in detail the experimental validation strategy. Chapter 5 shows the resulting experimental performance of the proposed method. Finally, Chapter 6 shows the conclusions and future remarks.

2. Problem Statement

Several authors have successfully employed an analytical model to estimate EV's Instantaneous Power Consumption (IPC) considering multiple vehicle and terrain parameters [2, 3]. This model explains how electric power is converted into tractive power (see Fig. 2.1 for a reference free body diagram), considering the effect of wheel-terrain interactions, fluid resistance and motor dynamics. According to this

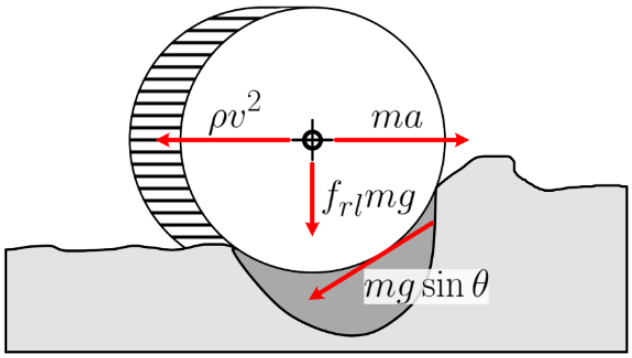

Figure 2.1.: Reference free body diagram of the wheel-terrain interaction.

model, IPC depends on the mass of the vehicle (which might vary in some applications, specially in public transportation systems [22, 26, 29]), the roughness of the terrain, its inclination, the rolling coefficient of the tire with respect to the terrain (it is not the same to traverse over gravel than over sand or grass, as reported in [2, 3, 20]), the aerodynamic drag coefficient, the deformability of the tire, the weight distribution on the vehicle, the inner and outer temperature, and vehicle's velocity and acceleration [2, 21, 30]. Additionally, vehicles have auxiliaries, which are defined as any other device that uses power from the vehicle batteries and are not associated with the motion of the vehicle, such as lights, air conditioning and on board computer, among others.

Following the guidelines presented in [2], the aforementioned analytical model of the IPC of an EV is obtained by relating electric motor equations with traction force. The traction force f_{tr} required by an EV can be modelled by Eq. 2.1, where m, a and v correspond to the mass, linear acceleration and linear velocity of the vehicle, respectively. The term R_A captures the effects of aerodynamic drag, with C_d and A_f denoting drag coefficient and frontal area of the vehicle, and ρ is air density. The wheel-terrain interaction is captured by the R_{RL} term, where g is gravitational acceleration and f_{rl} is the rolling coefficient, which depends on tire pressure and both terrain and tire composition. If the terrain presents an inclination θ, then a portion of the gravitational pull will be deviated from R_{RL} and captured by the term R_G. Note that Eq. 2.1 applies only to vehicles with non-deformable wheels performing linear motion, and is valid for both internal combustion engines and EVs. Additionally, the model assumes that wind speed is negligible; if this were not the

[2]: Wu et al. (2015), 'Electric vehicles' energy consumption measurement and estimation'

case, its value should be considered as an offset to v in the R_A term.

$$f_{tr} = ma + \underbrace{\frac{\rho}{2} C_d A_f v^2}_{R_A} + \underbrace{f_{rl} mg \cos\theta}_{R_{RL}} + \underbrace{mg \sin\theta}_{R_G} \tag{2.1}$$

The traction force f_{tr} and the motor torque τ can be related through traction power as shown in Eq. 2.2, where ω_m corresponds to the angular velocity of the motor's shaft and η_{dr} is the efficiency of the drive train.

$$P_{tr} = f_{tr} v = \tau \omega_m \eta_{dr} \tag{2.2}$$

For a brushed direct current (BDC) motor, input power is mainly converted to tractive power and resistive losses on its windings [2], as shown by Eq. 2.3, where R_a is the motor armature resistance, K is the motor torque constant and I_{in}, P_{in} refer to input current and power as seen in the motor terminals.

$$P_{in} = I_{in}^2 R_a + K I_{in} \omega_m \tag{2.3}$$

Note that an equivalent formulation can be obtained if current and voltage are taken from the input to the motor controller, by adding to R_a a resistance explaining power losses on this device [22].

For a BDC motor, torque is proportional to input current as shown in Eq. 2.4. Using Eq. 2.2 and taking into account wheel radius R and speed ratio r_{dr} of the drive train to relate linear and angular velocities, the input current can be expressed in terms of traction force as shown in Eq. 2.4.

$$\tau = K I_{in} = \frac{R}{r_{dr} \eta_{dr}} f_{tr} \tag{2.4}$$

Replacing this relation into Eq. 2.3, an analytical model of traction power of an EV is obtained in Eq. 2.5. Note that despite having assumed a BDC motor for this particular formulation, an analogous expression can be obtained for brushless direct current (BLDC) motors.

$$P_{tr} = \left(\frac{R}{K r_{dr}}\right)^2 R_a \left(\frac{1}{\eta_{dr}} f_{tr}\right)^2 + \frac{1}{\eta_{dr}} f_{tr} v \tag{2.5}$$

It is to be noted that a and v are time-dependent quantities; θ and f_{rl} are terrain dependent parameters and can change if the vehicle's path involves more than one terrain; R_A and K are known to suffer variations with temperature (see [22] for more details) and η_{dr} can be affected if the mechanical parts of the drive train are not properly maintained [3, 12, 21]. Although these variations are not considered in this work.

Instantaneous power consumption of an EV is mainly composed by traction power P_{tr}, required for vehicle's motion, and auxiliary power P_{aux} [21] consumed by other onboard systems. The modelling of auxiliary power lies out of the scope of this work, thus total power consumption P will be considered to be just traction power P_{tr}.

The proposed thesis will develop a method for estimating IPC of an EV based on the analytical model presented in Eq. 2.5, knowledge of the model parameters, and a set of inaccurate positioning data, with the goal of obtaining an estimate of average power consumption ($\frac{1}{N} \sum_k^N IPC_k$).

To achieve this, all vehicle and terrain parameters will be considered to remain constant, and non-accelerated linear motion will be assumed (see [22] for a detailed study of EV power consumption under different motion regimes) and EV's velocity will be estimated from a fixed-length queue of positioning data. Power consumption will be studied as a stochastic process as in [8, 9, 11, 30] (and the references therein), and its statistics and their relation to the velocity estimate will be fully characterized. From this knowledge, an optimization problem will be formulated to find an appropiate velocity estimate in order to obtain accurate power consumption estimates.

A general diagram of the presented problem is shown in Fig. 2.2. Briefly, a fixed-length queue of measurements is obtained from an inaccurate positioning data source. A velocity estimate is computed from this data and an IPC estimate is generated. Once the path is completed, average power consumption is computed and fed to Route Planning Systems.

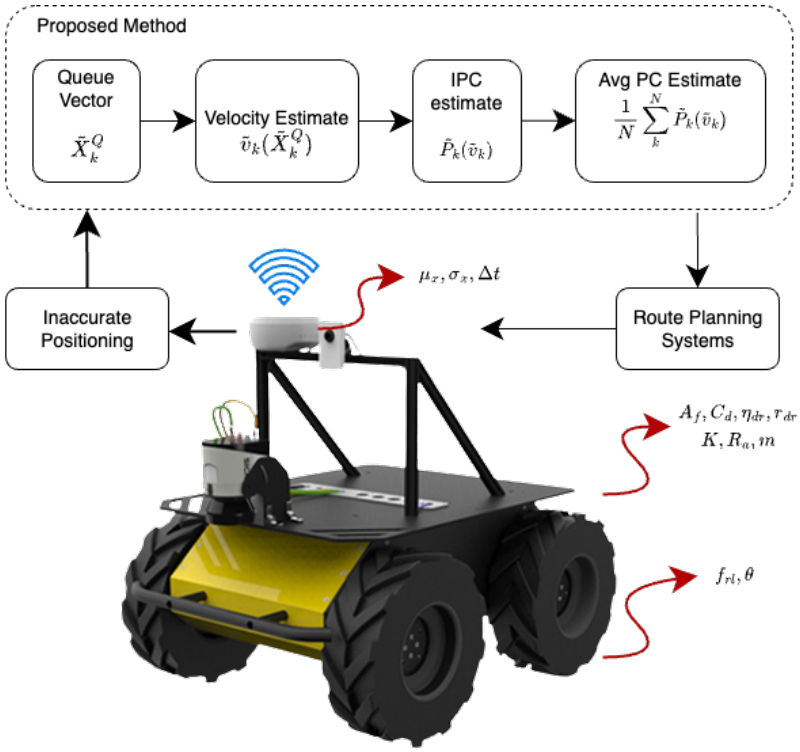

Figure 2.2.: General overview of the presented problem: to accurately estimate the IPC from an EV from inaccurate positioning data.

In the following sections -unless stated otherwise- matrices will be written in uppercase letters, vectors in boldface lowercase and scalars in lowercase letters. Every vector is a column vector, a vector with all entries equal to 1 will be denoted by $\mathbf{1}$, and a vector whose i-th entry is equal to 1 and all other entries are equal to 0 will be denoted by $\mathbf{1}_i$.

Matrix and vector dimensions -if not made explicit- can be inferred from context. The vector corresponding to the i-th row and column of a matrix will be denoted with matrix notation and subscript "$(i,:)$" and "$(:,i)$" respectively. The scalar corresponding to the i-th element of a vector will be denoted with vector notation and subscript "i".

The usual inner product for real-valued vectors will be denoted by $\langle \cdot, \cdot \rangle$. Vector or matrix transposition is denoted by $(\cdot)^T$.

3. Proposed Method

3.1. Stochastic approach to IPC estimation

As shown in Eq. 2.5, the IPC depends on vehicle velocity and acceleration. For the purposes of this work, velocity changes will be assumed to be sufficiently smooth, such that acceleration in Eq. 2.5 can be discarded and f_{rl} can be considered constant as shown in [2, 3, 20, 21]. Let Eq. 3.1 be an estimator for vehicle velocity, with v_k the true velocity at time $t = t_0 + k\Delta\, t$ and $\gamma_{v,k}$ a zero-mean Gaussian process of known variance σ_v^2 modelling estimation error.

$$\tilde{v}_k = v_k + \gamma_{v,k} \tag{3.1}$$

Further, let's assume that terrain angle variations are sufficiently small, such that θ is approximately constant. Under this assumption, the IPC can be estimated as

$$P_{tr}(\tilde{v}_k) \triangleq \widetilde{P}_k = K_m(K_a\tilde{v}_k^2 + K_t)^2 + (K_a\tilde{v}_k^2 + K_t)\tilde{v}_k, \tag{3.2}$$

where

$$K_t = \frac{1}{\eta_{dr}}\left(f_{rl}mg\cos\theta + mg\sin\theta\right), \tag{3.2a}$$

$$K_m = \left(\frac{R}{Kr_{dr}}\right)^2 R_a, \tag{3.2b}$$

$$K_a = \frac{\rho}{2\eta_{dr}} C_d A_f. \tag{3.2c}$$

To analyse the statistical performance of the proposed estimator, we first note that the moments of a Gaussian, zero-mean, random variables are characterized by the closed expression presented in Eq. 3.3,

$$\mathbb{E}\{\gamma_{v,k}^p\} = \begin{cases} 0 & \text{if } p \text{ is odd,} \\ \sigma_v^p(p-1)!! & \text{if } p \text{ is even.} \end{cases} \tag{3.3}$$

where !! stands for double factorial operation. Applying Eq. 3.3, both the mean and variance of the proposed estimator can be written as a function of the velocity's estimate variance σ_v^2 as shown in Eqs. 3.4 and 3.5, respectively.

$$\begin{aligned} \mu_{\widetilde{P}} &= \mathbb{E}\{\widetilde{P}_k\} = P_k + B_k \\ B_k &= K_a\sigma_v^2\left(K_mK_a(\sigma_v^2 + 6v_k^2) + 3v_k + 2K_mK_t\right) \end{aligned} \tag{3.4}$$

Equation 3.4 indicates that the proposed IPC estimator $\widetilde{P}_k$ is biased, since the bias term B_k depends on the vehicle's current velocity v_k and velocity's estimate variance σ_v^2, both non-zero quantities under the

assumptions of this work.

$$\sigma_{\text{P}}^2 = \mathbb{E}\left\{ \left(\widetilde{P}_k - \mu_{\text{P}} \right)^2 \right\} = c_1 \sigma_v^6 + c_2 \sigma_v^4 + c_3 \sigma_v^2 \tag{3.5}$$

$$c_1 = (4K_m K_a^2 v_k + K_a)^2 \tag{3.5a}$$

$$\begin{aligned} c_2 = {} & 2(4K_m K_a^2 v_k + K_a)(4K_m K_a^2 v_k^3 + 3K_a v_k^2 \\ & + 4K_m K_t K_a v_k + K_t) \end{aligned} \tag{3.5b}$$

$$c_3 = (4K_m K_a^2 v_k^3 + 3K_a v_k^2 + 4K_m K_t K_a v_k + K_t)^2 \tag{3.5c}$$

Note that coefficients c_1, c_2, c_3 depend not only on K_t, K_m, and K_a, but also on the true velocity of the vehicle at any sampling time. An important fact arises from this analysis: both bias and variance of the proposed estimator are directly proportional to σ_v^2.

3.2. A general velocity estimate

Let us now elaborate on the specific structure of the velocity estimator. As the only information available –aside from knowledge of vehicle, terrain and sensor parameters– is the output of an arbitrary localization system, velocity must be estimated from position samples. To this end, we define a *queue vector* $\widetilde{\mathbf{X}}_k^{\text{Q}} \in \mathbb{R}^{\text{Q}+1}$ with position samples, where the *queue size* Q corresponds to the number of past samples queued in $\widetilde{\mathbf{X}}_k^{\text{Q}}$. Samples in this vector are ordered such that $\tilde{x}_1$ and $\tilde{x}_{\text{Q}+1}$ are the first and last elements of $\widetilde{\mathbf{X}}_k^{\text{Q}}$ and correspond to the newest and oldest samples available, respectively. Queue vector $\widetilde{\mathbf{X}}_k^{\text{Q}}$ can be further decomposed as $\widetilde{\mathbf{X}}_k^{\text{Q}} = \mathbf{X}_k^{\text{Q}} + \mathbf{\Gamma}_{x,k}^{\text{Q}}$, where $\mathbf{X}_k^{\text{Q}}$ and $\mathbf{\Gamma}_{x,k}^{\text{Q}}$ contain the corresponding true position and measurement error on each sample. Additionally, $\mathbf{\Gamma}_{x,k}^{\text{Q}}$ entries are assumed to be Gaussian independent and identically distributed (i.i.d.) random variables with zero mean and σ_x^2 variance. Based on these definitions, the following velocity estimator is proposed:

$$\tilde{v}_k = \frac{1}{\Delta t} \mathbf{\Phi}^T \widetilde{\mathbf{X}}_k^{\text{Q}} = \underbrace{\frac{1}{\Delta t} \mathbf{\Phi}^T \mathbf{X}_k^{\text{Q}}}_{v_k} + \underbrace{\frac{1}{\Delta t} \mathbf{\Phi}^T \mathbf{\Gamma}_{x,k}^{\text{Q}}}_{\gamma_{v,k}}, \tag{3.6}$$

where $\mathbf{\Phi}$ is a vector of appropriate dimensions such that $\Delta t^{-1} \mathbf{\Phi}^T \mathbf{X}_k^{\text{Q}}$ constitutes a discrete linear approximation of continuous time derivation. Note that by the assumptions imposed to $\mathbf{\Gamma}_{x,k}^{\text{Q}}$, the term $\mathbf{\Phi}^T \mathbf{\Gamma}_{x,k}^{\text{Q}}$ is a Gaussian random variable of zero mean with σ_v^2 variance.

$$\begin{aligned} \mu_v &= \mathbb{E}\{\tilde{v}_k\} = \frac{1}{\Delta t} \mathbf{\Phi}^T \mathbf{X}_k^{\text{Q}} \\ \sigma_v^2 &= \frac{1}{\Delta t^2} \mathbf{\Phi}^T \mathbb{E}\{\mathbf{\Gamma}_{x,k}^{\text{Q}} (\mathbf{\Gamma}_{x,k}^{\text{Q}})^T\} \mathbf{\Phi} = \frac{\mathbf{\Phi}^T \mathbf{\Phi}}{\Delta t^2} \sigma_x^2 \end{aligned} \tag{3.7}$$

Furthermore, $\tilde{v}_k$ satisfies Eq. 3.7, where σ_v^2 is given explicitly in terms of $\mathbf{\Phi}$, sampling interval Δt and σ_x^2. Note also that $\tilde{v}_k$ in Eq. 3.6 matches the previously assumed structure in Eq. 3.1. The computation of $\mathbf{\Phi}$ will be explained next.

3.3. Optimum velocity estimate from localization

In the previous section, $\mathbf{\Phi}$ was unspecified. Nevertheless, it must satisfy certain conditions in order to constitute an approximation to continuous time derivation. Herein, $\mathbf{\Phi}$ will be fully characterized by means of an optimization problem, formulated to minimize both bias and variance of the proposed IPC estimator, constrained by the localization system characteristics.

Assuming an homogeneous sampling interval $\Delta\, t$, a first order derivative will be approximated by a backward difference quotient (BDQ) of the form:

$$\frac{d}{dt}x(t)\bigg|_{t_0+k\Delta\, t} \approx \frac{x(t_0+k\Delta\, t)-x(t_0+(k-h)\Delta\, t)}{h\Delta\, t}. \tag{3.8}$$

To obtain a more general description of a BDQ from elements of the queue vector $\widetilde{\mathbf{X}}_k^{\mathrm{Q}}$, let us define the family of vectors $\mathbf{d}_j^i \subset \mathbb{R}^{\mathrm{Q}+1}$ as:

$$\mathbf{d}_j^i \triangleq \frac{\mathbf{1}_i - \mathbf{1}_j}{(j-i)}, \quad i<j \in [1, Q{+}1] \subset \mathbb{Z}, \tag{3.9}$$

where $\mathbf{1}_i$ is a vector of appropriate dimensions whose i–th element is 1 and the remaining are equal to zero. To correctly interpret the choice of indices, recall the ordering convention adopted for the elements of $\widetilde{\mathbf{X}}_k^{\mathrm{Q}}$ in Chapter 2. Note that any possible BDQ from $\widetilde{\mathbf{X}}_k^{\mathrm{Q}}$ can be written as:

$$\Delta\, t^{-1}\langle\, \mathbf{d}_j^i, \widetilde{\mathbf{X}}_k^{\mathrm{Q}}\rangle = \frac{\tilde{x}_i - \tilde{x}_j}{(j-i)\Delta\, t}. \tag{3.10}$$

Furthermore, the following property holds:

$$\mathbf{d}_\ell^k = \left(\frac{\ell-1}{\ell-k}\right)\mathbf{d}_\ell^1 - \left(\frac{k-1}{\ell-k}\right)\mathbf{d}_k^1, \tag{3.11}$$

where $1 < k < \ell \leq Q+1$. Thus, to form every BDQ it is enough to consider the elements of set:

$$\mathcal{D}_Q \triangleq \{\mathbf{d}_j^1 \mid j \in [2, Q+1]\}. \tag{3.12}$$

A linear, general velocity estimate $\tilde{v}_k$ is then structured as a weighted average of every possible BDQ obtained from queue vector $\widetilde{\mathbf{X}}_k^{\mathrm{Q}}$. Let $\mathbf{D}_Q$ be a rectangular Q×Q+1 matrix whose j–th row is given by the transpose of element $\mathbf{d}_j^1$ in set $\mathcal{D}_Q$. Hence, the proposed velocity estimate can be expressed as

$$\tilde{v}_k = \frac{1}{\Delta t}\mathbf{\Phi}^T\widetilde{\mathbf{X}}_k^{\mathrm{Q}}, \quad \mathbf{\Phi} = \mathbf{D}_Q^T\boldsymbol{\alpha}, \tag{3.13}$$

where $\boldsymbol{\alpha}$ satisfies $\sum \alpha_i$=1. For example, for $Q = 3$:

$$\mathbf{D}_3 = \begin{bmatrix} 1 & -1 & 0 & 0 \\ 1/2 & 0 & -1/2 & 0 \\ 1/3 & 0 & 0 & -1/3 \end{bmatrix} \tag{3.14}$$

As the expressions for IPC estimate bias (B_k in Eq. 3.4) and variance (Eq. 3.5) contain the unknown term v_k (corresponding to the true underly-

ing velocity of the vehicle), neither of them can be used as a cost function to compute $\mathbf{\Phi}$ by means of an optimization problem. Nevertheless, they share the same structure as polynomials of σ_v^2. Assuming, without loss of generality, that v_k is positive, then every coefficient in these polynomials is positive. Thus both bias and variance become monotonically decreasing functions as σ_v^2 decreases. Therefore, a reasonable approach to minimize both expressions is to use Eq. 3.15 as the cost function to minimize, with $\mathbf{A}$ as defined in Eq. 3.16. Furthermore, matrix $\mathbf{A}$ is symmetric and positive definite and Eq. 3.15 constitutes a convex quadratic form. Consequently, the resulting optimization presented in Eq. 3.17 is convex and linear. It is important to note that matrix $\mathbf{A}$ is known, fixed by the choice of queue size Q and full rank (see Eq. 3.18).

$$\mathbf{\Phi}^T\mathbf{\Phi} = \boldsymbol{\alpha}^T\mathbf{A}\boldsymbol{\alpha} \tag{3.15}$$

$$\mathbf{A} = \mathbf{D}_Q\mathbf{D}_Q^T \tag{3.16}$$

$$\boldsymbol{\alpha}^* = \arg\min_{\boldsymbol{\alpha}} \boldsymbol{\alpha}^T\mathbf{A}\boldsymbol{\alpha} \qquad \text{s.t.} \quad \sum_{i=1}^{Q} \alpha_i = 1 \tag{3.17}$$

$$\text{Rank}\{\mathbf{A}\} = \text{Rank}\{\mathbf{D}_Q\mathbf{D}_Q^T\} = \text{Rank}\{\mathbf{D}_Q\} = Q \tag{3.18}$$

A linear, convex and restricted optimization problem shares its solution with the simpler unconstrained Lagrangian dual problem:

$$\max_{\lambda}\min_{\boldsymbol{\alpha}} \mathcal{L}(\boldsymbol{\alpha},\lambda) = \boldsymbol{\alpha}^T\mathbf{A}\boldsymbol{\alpha} + \lambda\left(\sum_{i=1}^{Q}\boldsymbol{\alpha}_i - 1\right). \tag{3.19}$$

The inner minimization can be solved by setting $\nabla_{\boldsymbol{\alpha}}\mathcal{L} = 0$:

$$\nabla_{\boldsymbol{\alpha}}\mathcal{L} = 2\mathbf{A}\boldsymbol{\alpha} + \lambda\mathbf{1} = 0 \implies \boldsymbol{\alpha}^* = -\frac{\lambda}{2}\mathbf{A}^{-1}\mathbf{1} \tag{3.20}$$

As a result, the optimum value of $\boldsymbol{\alpha}$ is obtained in terms of λ. Replacing the obtained $\boldsymbol{\alpha}^*$ in the Lagrangian dual problem we obtain a simple polynomial maximization:

$$\max_{\lambda} \; -\frac{\lambda^2}{4}\mathbf{1}^T\mathbf{A}^{-1}\mathbf{1} - \lambda, \tag{3.21}$$

which can be solved by setting

$$\frac{d}{d\lambda}\mathcal{L}(\boldsymbol{\alpha}^*,\lambda) = 0 \tag{3.22}$$

obtaining the optimal λ and consequently characterizing the optimal $\boldsymbol{\alpha}$:

$$\lambda^* = -\frac{2}{\mathbf{1}^T\mathbf{A}^{-1}\mathbf{1}} \implies \boldsymbol{\alpha}^* = \frac{\mathbf{A}^{-1}\mathbf{1}}{\mathbf{1}^T\mathbf{A}^{-1}\mathbf{1}}. \tag{3.23}$$

From the solution to this optimization problem, the proposed generalized BDQ approximation of vehicle velocity (Eq. 3.13) from localization samples queued on $\widetilde{\mathbf{X}}_k^Q$ is given by:

$$\mathbf{\Phi}^* = \mathbf{D}_Q^T\alpha^* = \frac{\mathbf{D}_Q^T\mathbf{A}^{-1}\mathbf{1}}{\mathbf{1}^T\mathbf{A}^{-1}\mathbf{1}}. \tag{3.24}$$

In the following sections, $\mathbf{\Phi}^*$ will be referred simply as $\mathbf{\Phi}$.

3.4. The Effects of Queue Size

In the previous section, the proposed estimator for the IPC of an EV from localization data queued in $\widetilde{\mathbf{X}}_k^{\mathrm{Q}}$ was fully characterized in terms of a fixed queue size Q and sensor characteristics (i.e. sampling frequency $\Delta\, t^{-1}$ and accuracy σ_x^2). This section explores the effects of queue size Q on the resultant $\mathbf{\Phi}$ vector and σ_v^2. This analysis will serve to establish a criterion for selecting Q in terms of σ_x^2, $\Delta\, t$ and a target value of σ_v^2. To find an explicit relation between Q and σ_v^2 (see Eqs. 3.7 and 3.24) $\mathbf{A}^{-1}$ needs to be computed. Despite the usual complexities of solving for the inverse of a matrix of arbitrary size, the properties of $\mathbf{A}$ allow for a simple way to perform this operation. First note that the i–th row of matrix $\mathbf{D}_Q$ is given by,

$$\mathbf{D}_{(i,:)} = \left(\mathbf{d}_{i+1}^{1}\right)^T \tag{3.25}$$

and elements $a_{i,j}$ of matrix $\mathbf{A} = \mathbf{D}_Q\mathbf{D}_Q^T$ are characterized by:

$$a_{i,j} = \begin{cases} \frac{2}{i^2} & \text{for } i{=}j \\ \frac{1}{ij} & \text{for } i{\neq}j \end{cases},\ i,j \in [1,Q] \subset \mathbb{Z}. \tag{3.26}$$

Further, note that the i-th column of $\mathbf{A}^{-1}$ can be expressed as the solution to the linear equation system:

$$\mathbf{A}\left(\mathbf{A^{-1}}_{(:,i)}\right) = \mathbf{1}_i. \tag{3.27}$$

Let $\boldsymbol{\lambda} \in \mathbb{R}^{\mathrm{Q}}$ be an arbitrary vector, $\boldsymbol{\lambda}_i$ its i–th entry, and $I = [1,Q] \subset \mathbb{Z}$ a set of indices. Then, it follows from Eq. 3.26 that:

$$\sum_{j\in I} \boldsymbol{\lambda}_j a_{i,j} = \frac{2\boldsymbol{\lambda}_i}{i^2} + \frac{1}{i}\sum_{j\in\{I-i\}} \frac{\boldsymbol{\lambda}_j}{j} = \frac{\boldsymbol{\lambda}_i}{i^2} + \frac{1}{i}\sum_{j\in I} \frac{\boldsymbol{\lambda}_j}{j}. \tag{3.28}$$

By applying the above identity, and denoting the elements of $\mathbf{A}^{-1}$ by $a_{i,j}^{-1}$, the system of linear equations on Eq. 3.27 can be expressed as

$$\begin{cases} \sum_{j\in I} a_{i,j}a_{i,j}^{-1} = 1 \\ \sum_{j\in I} a_{k,j}a_{i,j}^{-1} = 0 \end{cases} \rightarrow \begin{cases} \frac{1}{i}c + \frac{1}{i^2}a_{i,i}^{-1} = 1 \\ \frac{1}{k}c + \frac{1}{k^2}a_{i,k}^{-1} = 0 \\ c = \sum_{j\in I} \frac{1}{j}a_{i,j}^{-1} \end{cases}, \tag{3.29}$$

with $k \in \{I - i\}$. Therefore

$$a_{i,i}^{-1} = i^2 - ci \tag{3.30}$$

$$a_{i,k}^{-1} = -kc \tag{3.31}$$

and:

$$c = \sum_{j\in I} \frac{1}{j}a_{i,j}^{-1} = i - c - \sum_{j\in I} c \implies c = i\frac{1}{Q+1}. \tag{3.32}$$

Consequently, an element-wise expression for $\mathbf{A}^{-1}$ is obtained:

$$\mathbf{a}_{(i,j)}^{-1} = \begin{cases} i^2\left(\frac{Q}{Q+1}\right) & \text{for } i{=}j \\ -ij\left(\frac{1}{Q+1}\right) & \text{for } i{\neq}j \end{cases}, i,j \in [1,Q] \subset \mathbb{Z}. \tag{3.33}$$

Building on this result, $\mathbf{D}_Q^T\mathbf{A}^{-1}\mathbf{1}$ and $\mathbf{1}^T\mathbf{A}^{-1}\mathbf{1}$ can be computed from Eq. 3.24, as shown in Eqs. 3.34-3.36.

$$\left(\mathbf{A}^{-1}\mathbf{1}\right)_i = \sum_{j\in I} a_{i,j}^{-1} = i^2 - i\left(\frac{Q}{2}\right) \tag{3.34}$$

$$\mathbf{1}^T\mathbf{A}^{-1}\mathbf{1} = \sum_{i\in I}\left(\mathbf{A}^{-1}\mathbf{1}\right)_i = \frac{Q(Q+1)(Q+2)}{12} \tag{3.35}$$

$$\left(\mathbf{D}_Q^T\mathbf{A}^{-1}\mathbf{1}\right)_i = \begin{cases} \sum_{i\in I}\frac{1}{i}\left(\mathbf{A}^{-1}\mathbf{1}\right)_i = \frac{Q}{2} & \text{for } i = 1 \\ \frac{-1}{i-1}\left(\mathbf{A}^{-1}\mathbf{1}\right)_{(i-1)} = \frac{Q}{2}\text{-}(i\text{-}1) & \text{for } i > 1 \end{cases} \tag{3.36}$$

Both cases presented in Eq. 3.36 are equivalent. Therefore, $\mathbf{\Phi}$ can be expressed in an element-wise notation as:

$$\mathbf{\Phi}_i = \frac{Q/2\text{-}(i\text{-}1)}{(Q+2)(Q+1)Q/12}, \tag{3.37}$$

where the dependence on Q has been made explicit. Finally, $\mathbf{\Phi}^T\mathbf{\Phi}$ is given by:

$$\mathbf{\Phi}^T\mathbf{\Phi} = \sum_{i=1}^{Q}\mathbf{\Phi}_i = \frac{6(3Q^3+2Q^2-8)}{Q^2(Q+1)(Q+2)^2}. \tag{3.38}$$

Observing that both bias and variance of the proposed IPC estimator (Eqs. 3.4 and 3.5) are polynomials on σ_v^2, a simple criterion to constrain these quantities is to set $\sigma_v^2 < 1$, thus reducing the effect of higher order terms. This criterion, along with Eqs. 3.7 and 3.38 will serve to select Q in terms of sensor accuracy and sampling rate (σ_x and $\Delta\, t^{-1}$ respectively). Algorithm 1 summarizes the iterative process to determine the queue size as described above.

Algorithm 1: Determine queue size Q from sensor characteristics.

```
Let Q be the queue size as defined in Sec. ??.
Set the initial value Q = 1.
Evaluate Φ^T Φ from (eq. 3.38).
while Φ^T Φ > Δt^2/σ_x^2 do
    Set Q = Q + 1
    Evaluate Φ^T Φ from (eq. 3.38).
end
```

4. Experimental Setup

4.1. Experimental platform

The experimental platform consisted of a Clearpath Husky A-200 mobile robot, depicted on figure 4.1, equipped with an Nvidia Jetson TX2 computing unit and a Vectornav VN-200 Inertial Measurement Unit (IMU), coupled with a high-sensitivity GNSS antenna. In the following, each of this components is presented in detail.

Figure 4.1.: The experimental platform: a Husky A-200 robot from Clearpath Robotics.

Robotic platform

The Husky A-200 robotic platform provides a low level controller, connected trough serial communication with the main computing unit. The low level controller is mainly in charge of motor speed control (through encoder-based wheel odometry feedback), and general robot status monitoring. In particular, electrical monitoring is provided by means of onboard voltage and current sensors located at each motor driver and the auxiliary outputs. This configuration is depicted in figure 4.2. The whole system is powered by a 24 volts 20 Ampere-hour sealed lead-acid battery, further regulated to provide 5, 12 and 24 volt outputs, each fused at 5A. These outputs are used to power the onboard electronics, such as the main computing unit and additional sensors.

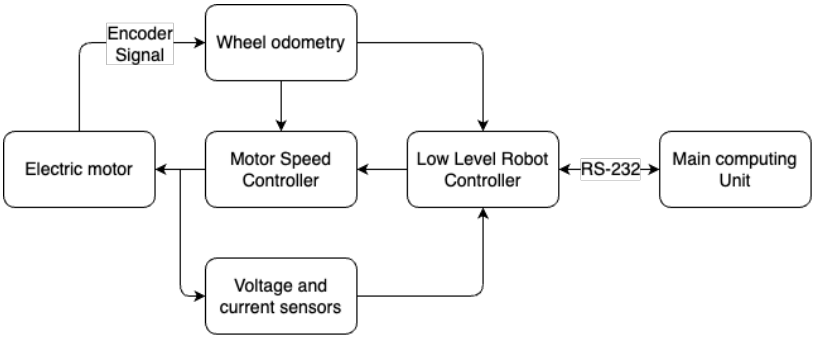

Figure 4.2.: Robotic platform low level controller overview.

The robotic platform is skid-steered, meaning that each side has its own motor, and steering is achieved by varying the wheel velocities between the left and right sides. A summary of the main robotic platform characteristics is presented in table 4.1.

Characteristic	**Value**
Dimensions	990 [mm] length 670 [mm] width 390 [mm] height
Track	555 [mm]
Wheelbase	512 [mm]
Ground clearance	130 [mm]
Weight	50 [kg]
Speed (max)	1 [m/s]
Communication	RS-232 115,200 [baud]
Wheel encoders	78,000 [ticks/m]
Battery	24 [v] 20 [Ah] sealed lead-acid
Electric motors	24 [v] DC 10.7 [A] with planetary gears

Table 4.1.: Summary of Husky A-200 robotic platform parameters, as reported on the corresponding user manual.

Additional hardware

The main computing unit, where all high level software is deployed, consists of an Nvidia Jetson TX2 developer kit mounted directly on the robotic platform (see fig. 4.3). This is a highly capable embedded platform, with an ARM based computing architecture designed for real-time performance on Artificial Intelligence and other computationally intensive applications. The developer kit comprises two main components: the carrier board and the processing module itself. The carrier board includes all the required connectors and interfaces for this work. The main characteristics of this device are presented in Table 4.2.

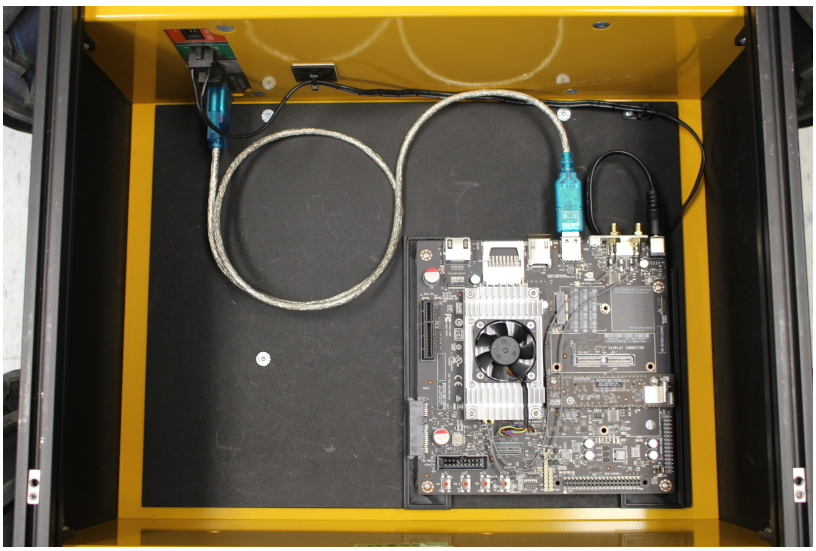

Figure 4.3.: Main computing unit: Nvidia Jetson TX2 developer kit mounted on the Husky A-200 robotic platform.

The only additional device connected to the main computing unit (besides the low level controller) is a Vectornav VN-200 IMU and GNSS receiver coupled with a high sensitivity GNSS antenna, as depicted in figure 4.4. This device provides X-Y-Z linear and angular acceleration estimates at 200 [Hz], as well as GNSS positioning at a 5 [Hz] rate. The main characteristics of this device are summarized in table 4.3.

Characteristic	Description
GPU	NVIDIA Pascal™with 256 CUDA cores
CPU	HMP Dual Denver 2 / 2 MB L2 Quad ARM®A57 /2 MB L2
Memory	8 GB 128 bit LPDDR4 59.7 GB/s

Table 4.2.: Summary of Nvidia Jetson TX2 characteristics, as reported by the manufacturer.

Figure 4.4.: Vectornav VN-200 IMU and GNSS receiver with its respective GNSS antenna.

Intertial Measurement Unit		
Characteristic	**Accelerometer**	**Gyroscope**
Range	± 16 [g]	± 2,000 [°/s]
In-run bias stability	< 0.04 [mg]	< 10 [°/hr]
Cross-axis sensitivity	± 0.05 [°]	< 0.05

GNSS Receiver	
Characteristic	Value
Receiver type	2 Channel, L1C/A, L1OF, E1, B1I GNSS
Constellations	GPS, Gallileo, SBAS
Time to first fix	29 [s]
Sensitivity	-159 [dBm]

Table 4.3.: Summary of Vectornav VN-200 accelerometer, gyroscope and GNSS receiver characteristics, as reported by the manufacturer.

4.2. Trial design

Experimental validation was performed inside the main campus of *Universidad Técnica Federico Santa María* (UTFSM), Valparaíso, Chile. The previously described robotic platform (with rubber tires) was used to perform a total of 54 trials, distributed evenly among three different terrains: grass, gravel and asphalt, at two different speeds: 0.4 and 1 [m/s]. The robot was set to follow a straight line while maintaining a constant speed. The specific location for each terrain is depicted on Fig. 4.5 and was chosen such that no significant inclination is observed. Tire pressure was controlled at the beginning of each trial maintaining a level of 15 psi at all times.

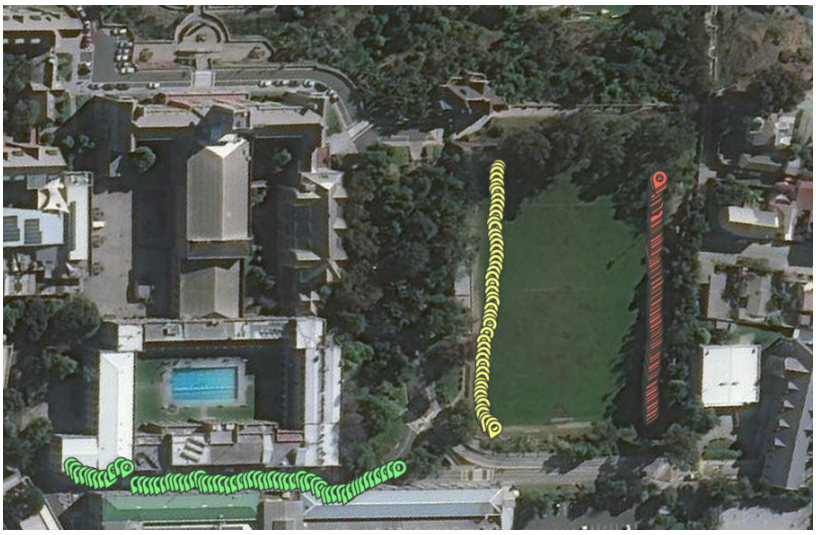

Figure 4.5.: Experimental site and GNSS waypoints from a particular trial of gravel, grass and asphalt (displayed on yellow, red and green waypoints respectively) at UTFSM Campus, Valparaíso, Chile.

4.3. Software components

The main computing unit (Jetson TX2) was installed with Ubuntu Linux 18.04 (Bionic). A Robot Operating System (ROS) distribution (Melodic Morenia) served as the base for the software architecture of this work. ROS is a middleware that operates on top of a conventional operating system to provide a framework and set of tools for developing robot applications. Particularly, it provides a node based process management solution (ROS nodes), a publisher/subscriber message based inter-process communication mechanism (ROS topics) and a data recording solution (ROS bags).

ROS is widely adopted on the robot development community, and ClearPath Robotics provides official ROS driver nodes for the Husky A-200 robot. These nodes are used to interface with the low level controller to set motor speed control set point, and read relevant robot status information: voltage and current from each motor controller and wheel encoder odometry, among other information not relevant to this work.

Similarly, there's an official ROS driver node for the Vectornav VN-200 IMU and GNSS system. This node is used to obtain readings from GNSS positioning and IMU (three-axis accelerometer and gyroscope).

As part of the Robot Localization Package [31], ROS provides an Extended Kalman Filter (EKF) implementation node, further configured by the robotic platform manufacturer. This node is used to estimate vehicle position and velocity by fusing readings from wheel odometry from the robot's encoders with IMU data from the Vectornav sensor. EKF parameters were kept on their default values as delivered by the robotic platform manufacturer. Note that GNSS data is not fused into this estimate.

Finally, a ROS bag node is used to record GNSS positioning and EKF velocity and position estimates during trials. Electrical monitoring data is also recorded, including voltage and current measurements reported by the robot for each motor. Although they have been found to be non-accurate and other authors have dismissed them in favour of a custom monitoring system [22], these sensors will serve well for the purposes of

this work, as their mean values for each trial are the variable of interest. Figure 4.6 describes the complete software architecture for this work.

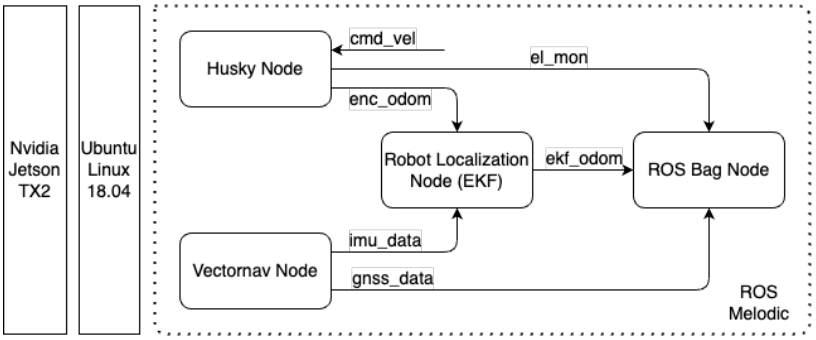

Figure 4.6.: Experimental platform software overview.

4.4. Data pre-processing

Data recorded during each trial is processed independently. Each trial's data comprises four main series: electrical monitoring (recorded at 1 [Hz]), GNSS positioning (recorded at 5 [Hz]), and EKF positioning † and velocity (both recorded at 200 [Hz]).

†: EKF positioning corresponds to the position estimate from the Extended Kalman Filter fusing wheel encoder odometry and Inertial Measurement Unit outputs.

As a first preprocessing step, all data points corresponding to the acceleration and deceleration stages at the beginning and end of each trial are discarded (recall that, for the purposes of this work, non-accelerated linear motion is assumed). To this end, the first and last segments of the data where EKF velocity estimate is lower than 0.4 [m/s] are discarded.

GNSS positioning data is read in latitude, longitud and altitude format. Assuming that altitude is relatively constant through the experimental site, this variable is discarded from anaylsis. Latitude and longitude are converted from geodesic coordinates to cartesian coordinates on a local plane assuming that radius of the earth is approximately constant through the experimental site. This is known as the East, North, Up (ENU) or local tangent plane coordinate system (depicted in figure 4.7). Finally, the first data point is considered to be the origin of the local plane, and all resulting data points are shifted accordingly.

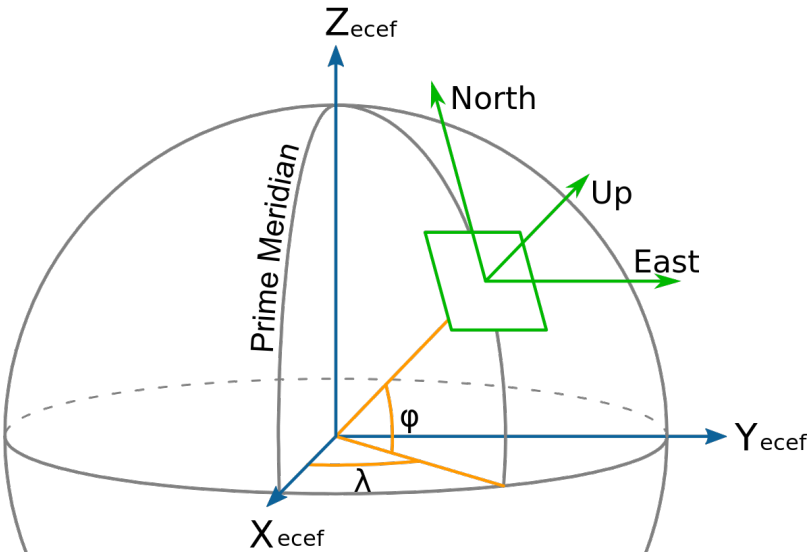

Figure 4.7.: Depiction of different spatial reference coordinate systems typically used in the context of GNSS positioning.

EKF positioning and velocity data are synchronized to GNSS positioning data, thus adopting the slowest sampling rate. EKF positioning data is also shifted by assuming that the first data point corresponds to the origin of the local coordinate system.

Note that the problem formulation presented in Chapter 2 considers motion on a single direction. Therefore, dimensionality of both positioning sources needs to be reduced to the corresponding direction of motion. This direction is characterized independently for each trial and source by the vector corresponding to the principal component resulting from a Principal Component Analysis (PCA) of the data. Each data source is projected onto this vector. An example of this procedure is presented in figure 4.8, particularly considering GNSS data samples.

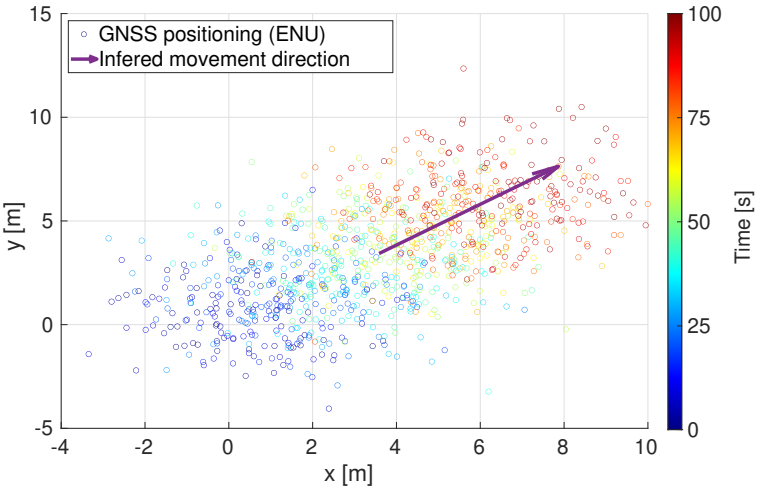

Figure 4.8.: Depiction of PCA-based characterization of the direction of motion.

Finally, electrical monitoring consists itself of four signals: left and right motors currents and voltages. Thus, experimental tractive power for each trial is estimated as the sum of the products of voltage and current from each motor. The average power consumption estimated from the resulting signal will serve as ground truth for each trial.

5. Experimental Results

5.1. Trials summary

The 54 trials were conducted in groups of 9 trials for each combination of speed and terrain. Table 5.1 summarizes the average distance, tractive power and speed for each group of trials. Distance and speed are taken from the EKF estimate. Only 900 data points were considered for trials performed at a target speed of 0.4 (m/s) and 450 for those at 1 (m/s), dismissing data corresponding to the acceleration and de-acceleration steps at the beginning and end of each trial.

Terrain	**Avg. Speed** (m/s)	**Distance** (m)	**Avg. Power** (W)
Grass	0.39 ± 0.00 0.96 ± 0.04	71.74 ± 0.15 88.99 ± 0.7	78.79 ± 5.59 102.03 ± 2.95
Gravel	0.39 ± 0.01 0.96 ± 0.03	71.24 ± 0.65 89.11 ± 0.48	54.14 ± 3.64 79.66 ± 4.51
Asphalt	0.38 ± 0.02 0.95 ± 0.04	71.45 ± 0.41 88.92 ± 0.71	47.06 ± 1.52 75.49 ± 3.57

Table 5.1.: Distance, average power and average speed for each group of trials.

The following figures 5.1, 5.2 and 5.3 showcase experimental positioning averaged along the 9 trials of each terrain and speed. Note that the difference between EKF and GNSS positioning becomes more apparent on asphalt than on gravel, and on gravel than on asphalt.

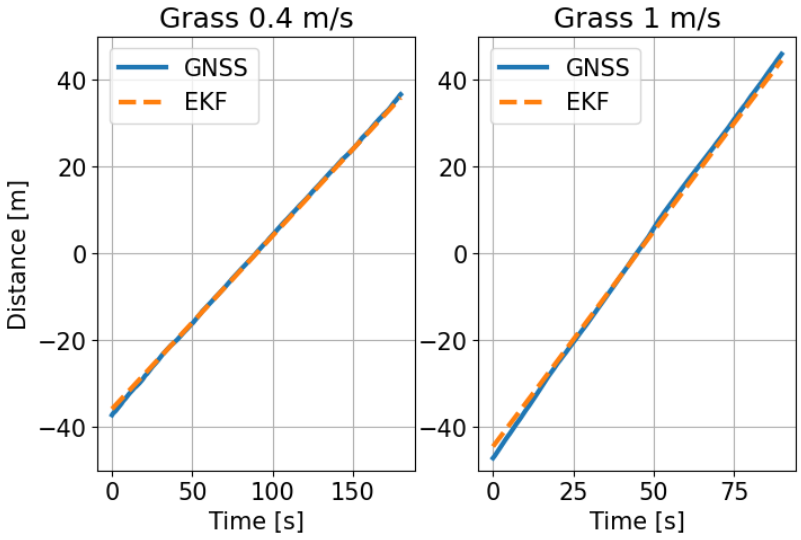

Figure 5.1.: Trials summary: average EKF and GNSS positioning for grass trials.

The following figures 5.4 and 5.5 showcase experimental tractive power averaged along the 9 trials of each terrain and speed. Note that, at both speeds grass requires more tractive power for displacement than gravel, and gravel than asphalt. Naturally, more tractive power is required at higher speed.

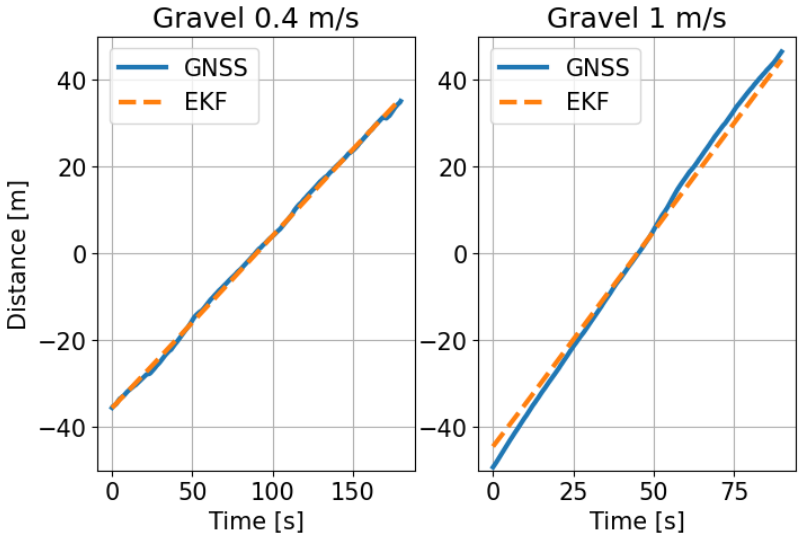

Figure 5.2.: Trials summary: average EKF and GNSS positioning for gravel trials.

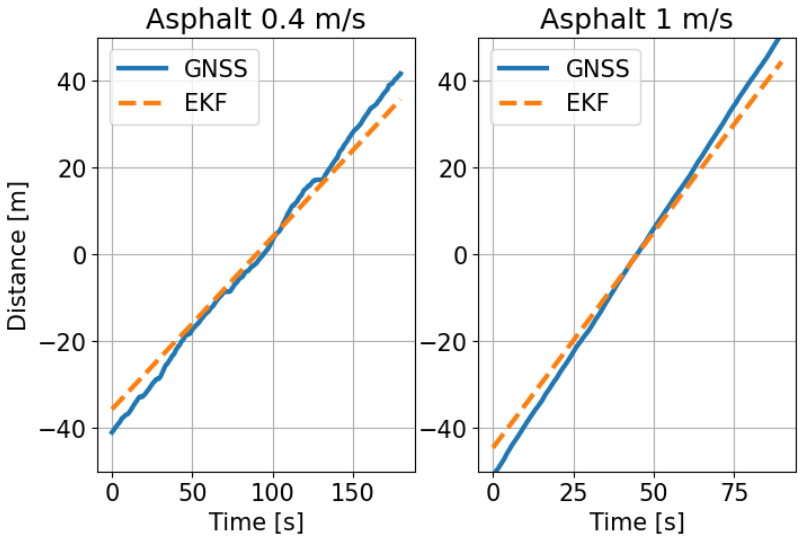

Figure 5.3.: Trials summary: average EKF and GNSS positioning for asphalt trials.

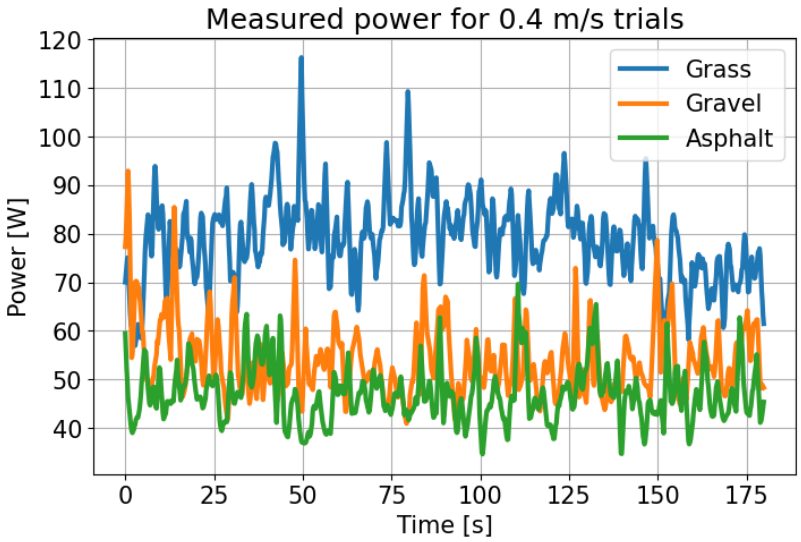

Figure 5.4.: Trials summary: average power for 0.4 m/s trials.

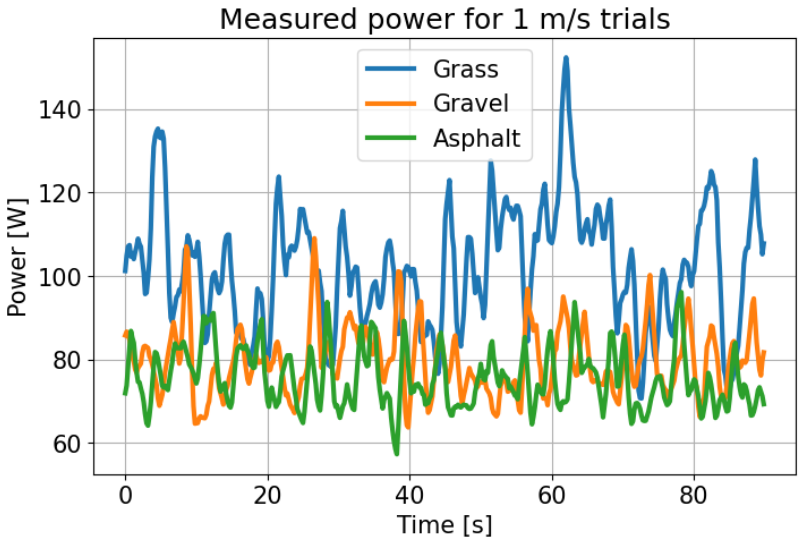

Figure 5.5.: Trials summary: average power for 1 m/s trials.

5.2. Parameter identification

The parameters K_a, K_m and K_t in Eq. 3.2, are estimated by numerical approximation to the solution of the system of non-linear equations given by:

$$P_{tr}(\bar{v}_i) = \bar{P}_i = K_m(K_a\bar{v}_i^2 + K_t)^2 + (K_a\bar{v}_i^2 + K_t)\bar{v}_i,$$

where $\bar{P}_i$ and $\bar{v}_i$ are the mean tractive power and mean speed of the i–th trial, respectively, over the 54 trials. Resulting parameters are presented in Tab. 5.2. Note that K_t is allowed to be changed for each terrain. The achieved fit results in the experimental and predicted power are presented in Fig. 5.6 for each trial.

Terrain	K_a	K_t	K_m
Grass		4.56	
Gravel	0.93	3.84	3.37
Asphalt		3.67	

Table 5.2.: Model parameters estimated from experimental data.

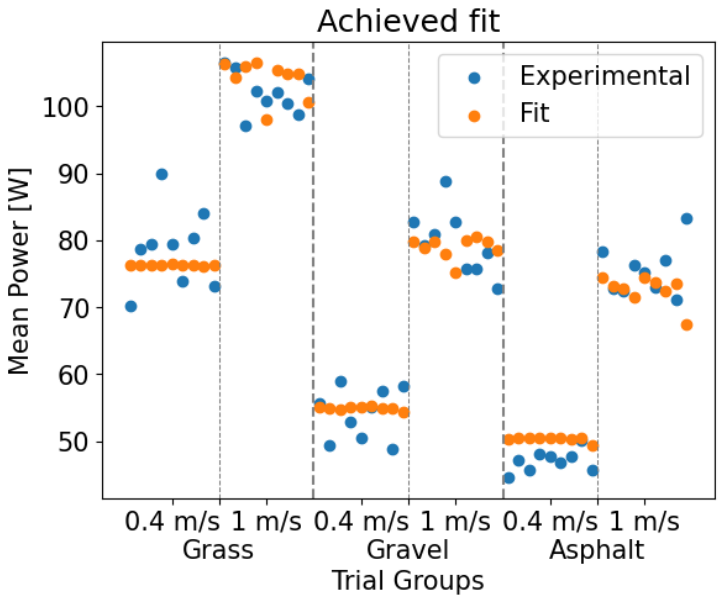

Figure 5.6.: Tractive power achieved fit for grass, gravel and asphalt.

In order to compute GNSS localization error (and its statistics), EKF estimates are assumed to be both accurate and precise relative to GNSS data. In other words, GNSS error assumes EKF estimates as ground-truth. The localization error is then computed as the difference between GNSS and EKF positioning data. Error statistics are computed over each group of 9 trials, obtaining the results presented in table 5.3.

Terrain	**Speed (m/s)**	**Mean** (m)	**Std. Dev.** (m)
Grass	0.4	1.80	1.12
	1	2.62	1.37
Gravel	0.4	0.29	1.45
	1	4.68	2.74
Asphalt	0.4	7.16	4.23
	1	8.98	3.88

Table 5.3.: GNSS localization error statistics, computed by considering EKF localization estimates as ground truth.

Note that the assumption of a zero mean error does not hold for the experimental data, with asphalt being the worst case in terms of error mean. GNSS error distribution is known to change if the line of sight between the GNSS receiver antenna and the satellite constellations is interrupted. In fact, figure 5.7 shows a progressive distribution degradation between grass, gravel and asphalt, with grass and gravel (to some extent) being similar to a gaussian distribution, and asphalt presenting a more uniform distribution. As it can be seen in figure 4.5, grass trials were conducted with a clear line of sight to satellite constellations, gravel trials were obstructed by foliage, and asphalt trials were conducted in between two buildings, having a greater impact on line of sight.

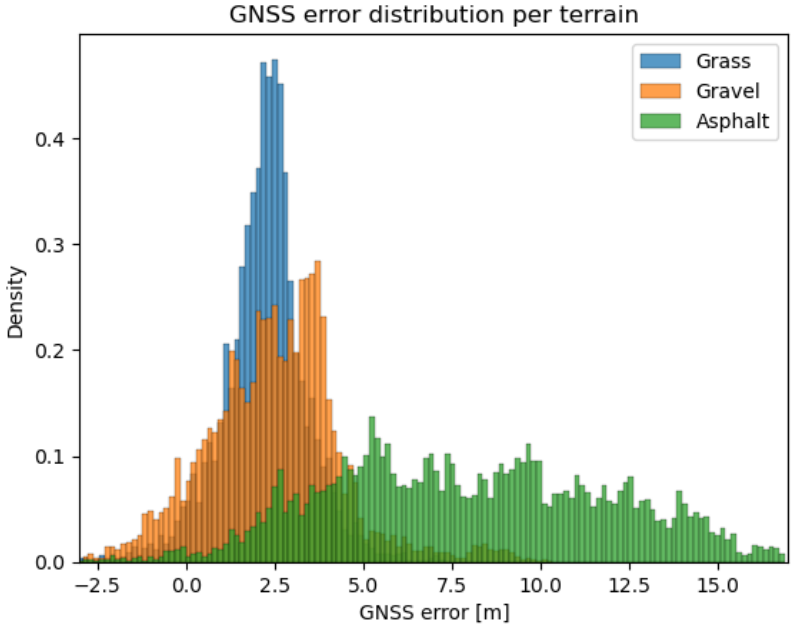

Figure 5.7.: GNSS error distribution as a function of the terrain.

5.3. Performance evaluation

Applying the proposed methodology and using queue size Q from Alg. 1, tractive power is estimated from GNSS localization data, as shown by Fig. 5.8 in blue bars, where mean and variance of the resulting estimate

are compared to those obtained from direct evaluation of velocity as reported by the EKF on the tractive power model (Eq. 3.2) in orange bars, and power computed directly from the electrical monitoring system in yellow bars.

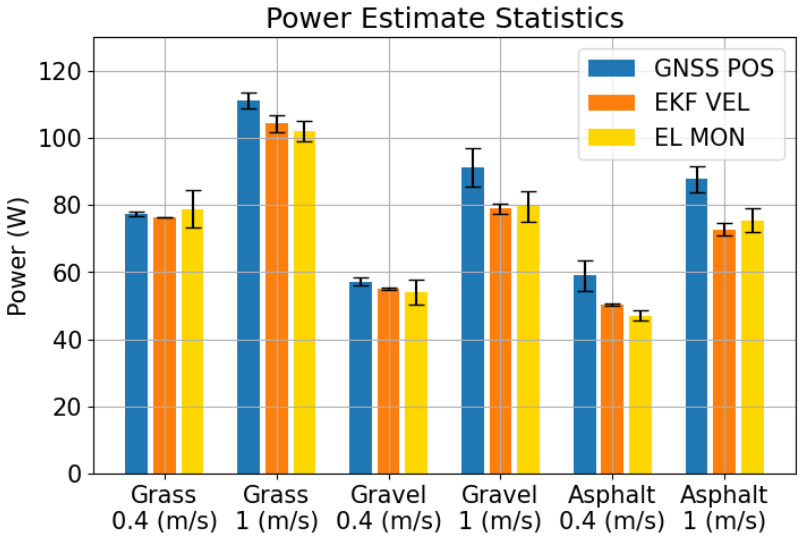

Figure 5.8.: Tractive power estimate statistics from three different sources: power model evaluated with EKF velocity in orange; the proposed methodology applied to GNSS localization in blue; and direct computation from electrical monitoring system in yellow bar.

By considering power derived from electric monitoring as ground truth, overall performance of the proposed estimator is presented in Tab. 5.4 in terms of percentage error of the mean tractive power per terrain and speed, as defined in Eq. 5.1,

$$P_{acc} = \left(1 - \frac{|P_{est} - P_{true}|}{P_{true}}\right) * 100. \tag{5.1}$$

Table 5.4.: Mean power per terrain and speed, obtained from evaluation of the tractive power model with EKF velocity and GNSS localization estimate using the proposed method.

Terrain	**Vel (m/s)**	**EL MON** (W)	**GNSS POS** (W)	**Acc** (%)	**EKF VEL** (W)	**Acc** (%)
Grass	0.4	78.79	77.39	98.22	76.29	96.83
	1	102.03	111.06	91.15	104.21	97.86
Gravel	0.4	54.14	57.24	94.27	54.98	98.45
	1	79.66	91.23	85.48	79.01	99.18
Asphalt	0.4	47.06	58.95	74.73	50.37	92.97
	1	75.49	87.69	83.84	72.75	96.37

The EKF VEL estimate has a consistent performance across different terrains and speeds: the worst case accuracy observed for this estimate is 92.97%. Recall that this estimate is obtained by evaluating the velocity estimate from the Extended Kalman Filter fusing IMU measurements and wheel encoders on the tractive power model presented in Eq. 3.2. This is done by using the parameters identified experimentally in the previous section. Therefore, this result validates the tractive power modelling and parameter identification procedure and any limitations in performance of the GNSS POS estimate are not related to them.

On the other hand, GNSS POS power estimate accuracy degrades from grass to gravel and asphalt, with a 98.22% and 74.73% best and worst case scenario respectively. It should be noted that worst case scenario is observed with highly inaccurate positioning: $\sigma_x^2 \approx 18$ m in the 0.4

m/s trials on asphalt. This result is consistent with the increase in GNSS positioning error standard deviation presented in Table 5.7 when transtioning from grass to gravel and asphalt.

To better understand the performance of the proposed method, baseline accuracy is determined estimating velocity from GNSS positioning by taking the naive two-point derivative approximation instead of the proposed method. The results are presented in Table 5.5. The proposed method consistently outperforms the baseline method. On average, the proposed method improves the baseline accuracy by 9.46%. Best case is 36.52% and worst case is -0.9%.

Terrain	**Vel (m/s)**	**BL Acc** (%)	**PM Acc** (%)	**Variation** (%)
Grass	0.4	99.12	98.22	-0.9
	1	89.72	91.15	1.43
Gravel	0.4	89.58	94.27	4.69
	1	78.3	85.48	7.18
Asphalt	0.4	38.21	74.73	36.52
	1	76.0	83.84	7.84

Table 5.5.: Accuracy of baseline (BL) and proposed method (PM) per terrain and speed, both obtained from evaluation of the tractive power model with GNSS positioning data.

6. Conclusions

6.1. Discussion

In this thesis, the problem of estimating the average power consumption of an electric vehicle from inaccurate positioning data is addressed. The proposed method is based on a widely adopted and validated phenomenological model of tractive power as a function of the vehicle's velocity. Our experimental results show that evaluating this model with an accurate velocity estimate (EKF velocity)† yields, on average, a power estimate accuracy of 97%. Thus, the main challenge in this work is to provide a good velocity estimate from inaccurate positioning data.

†: EKF velocity refers to the velocity estimate obtained by fusing wheel encoder odometry and Inertial Measurement Unit (IMU) outputs with an Extended Kalman Filter

This challenge was tackled by studying the propagation of positioning error through a general velocity estimate and its impact on the resulting tractive power estimate. This knowledge was then used to derive an optimal velocity estimate, such that the resulting power estimate exhibits minimal bias and variance. This method proved to yield significant improvements over the naive two-point velocity-from-position estimate, with an average accuracy improvement of nearly 10%. However, there is still room for improvement, as the EKF-based velocity estimate outperforms the proposed method by an additional 10% in the experimental results. This gap in performance needs to be analyzed carefully.

Experimental validation was conducted using a GNSS localization system as the source of inaccurate positioning data. GNSS localization has well-known limitations: data discontinuities (also known as discrete jumps), correlation of localization error with the surrounding architecture, and localization error that is poorly characterized by a Gaussian distribution when the line of sight to satellite constellations is disrupted.

Note that during the formulation of the proposed estimate, zero-mean Gaussian-distributed positioning error was assumed. Therefore, GNSS localization poses a worst-case scenario for the proposed estimator, and the observed experimental performance is highly constrained by this situation, particularly in the results from the asphalt trials.

Despite the aforementioned limitations, the results shown in Fig. 5.8 strongly suggest that average power consumption is correctly estimated, even in the presence of highly inaccurate positioning, thus validating the proposed method.

6.2. Future Work

The proposed method takes a step toward a reliable estimation of power consumption in the absence of electrical monitoring sensors, using only commonly available localization data sources (e.g., the GNSS receiver on a smartphone).

The results obtained encourage further investigation into this subject, particularly by extending the proposed method to the more general case

of a vehicle following paths with changes in slope, direction, and terrain composition. The good performance of the estimator also suggests a possible extension of the analysis to estimating the battery's state of charge using only localization data.

Appendix

Symbols table A.

Table A.1 describes the symbols used in this work.

Table A.1.: List of mathematical symbols and their corresponding description.

Symbol	Description
f_{tr}	Traction force required by the vehicle.
m	Vehicle's mass.
a	Vehicle's linear acceleration.
v	Vehicle's linear velocity.
x	Vehicle's position.
ρ	Air density.
C_d	Vehicle's drag coefficient.
A_f	Vehicle's frontal area.
g	Gravitational acceleration constant.
f_{rl}	Rolling coefficient.
θ	Terrain inclination.
P_{tr}	Traction power required by the vehicle.
τ	Motor torque
ω_m	Angular velocity of the motor shaft.
η_{dr}	Drive train efficiency.
P_{in}	Motor input electrical power.
I_{in}	Motor input electrical current.
R_a	Motor armature resistance.
K	Motor torque constant.
r_{dr}	Drive train speed ratio.
$\tilde{x}_k$	Notation for the estimate of quantity x at instant k.
x_k	Notation for the value of quantity x at instant k.
$\gamma_{x,k}$	Notation for the estimation error of quantity x at instant k.
μx	Notation for the mean of the estimator for quantity x.
σx	Notation for the variance of the estimator for quantity x.
$\widetilde{\mathbf{X}}_k^Q$	Queue vector, containing position samples.
Q	Queue size.
Δt	Sampling interval.

Bibliography

[1] Isaac Skog and Peter Händel. 'Indirect instantaneous car-fuel consumption measurements'. In: *IEEE Transactions on Instrumentation and Measurement* 63.12 (2014), pp. 3190–3198 (cited on page 1).

[2] Xinkai Wu et al. 'Electric vehicles' energy consumption measurement and estimation'. In: *Transportation Research Part D: Transport and Environment* 34 (2015), pp. 52–67 (cited on pages 1, 2, 4, 5, 7).

[3] Seongpil Cheon and Suk-Ju Kang. 'An electric power consumption analysis system for the installation of electric vehicle charging stations'. In: *Energies* 10.10 (2017), p. 1534 (cited on pages 1, 2, 4, 5, 7).

[4] Yanhai Xiong, Bo An, and Sarit Kraus. 'Electric vehicle charging strategy study and the application on charging station placement'. In: *Autonomous Agents and Multi-Agent Systems* 35 (2021), pp. 1–19 (cited on page 1).

[5] Arnab Pal, Aniruddha Bhattacharya, and Ajoy Kumar Chakraborty. 'Allocation of electric vehicle charging station considering uncertainties'. In: *Sustainable Energy, Grids and Networks* 25 (2021), p. 100422 (cited on page 1).

[6] Diego Iannuzzi and Pasquale Franzese. 'Ultrafast charging station for electrical vehicles: Dynamic modelling, design and control strategy'. In: *Mathematics and Computers in simulation* 184 (2021), pp. 225–243 (cited on pages 1, 2).

[7] Wenjuan Zhou and Li Wang. 'The Energy-Efficient Dynamic Route Planning for Electric Vehicles'. In: *Journal of Advanced Transportation* 2019.1 (2019), p. 2607402 (cited on page 1).

[8] Jen-Chiun Guan, Bo-Chiuan Chen, and Yuh-Yih Wu. 'Design of an adaptive power management strategy for range extended electric vehicles'. In: *Energies* 12.9 (2019), p. 1610 (cited on pages 1, 6).

[9] Jiuyu Du et al. 'Design method of a power management strategy for variable battery capacities range-extended electric vehicles to improve energy efficiency and cost-effectiveness'. In: *Energy* 121 (2017), pp. 32–42 (cited on pages 1, 6).

[10] Chiara Fiori et al. 'Energy consumption modeling in presence of uncertainty'. In: *IEEE Transactions on Intelligent Transportation Systems* 22.10 (2020), pp. 6330–6341 (cited on page 1).

[11] Hongwei Liu et al. 'An adaptive-equivalent consumption minimum strategy for an extended-range electric bus based on target driving cycle generation'. In: *Energies* 11.7 (2018), p. 1805 (cited on pages 1, 6).

[12] Javier Romero Schmidt and Fernando Auat Cheein. 'Prognosis of the energy and instantaneous power consumption in electric vehicles enhanced by visual terrain classification'. In: *Computers & Electrical Engineering* 78 (2019), pp. 120–131 (cited on pages 1, 2, 5).

[13] Zhaolong Zhang et al. 'Energy consumption prediction of electric vehicles based on digital twin technology'. In: *World Electric Vehicle Journal* 12.4 (2021), p. 160 (cited on page 1).

[14] Jose del C Julio-Rodríguez, Alfredo Santana-Díaz, and Ricardo A Ramirez-Mendoza. 'Individual drive-wheel energy management for rear-traction electric vehicles with in-wheel motors'. In: *Applied Sciences* 11.10 (2021), p. 4679 (cited on page 1).

[15] Teng Liu et al. 'Driving conditions-driven energy management strategies for hybrid electric vehicles: A review'. In: *Renewable and Sustainable Energy Reviews* 151 (2021), p. 111521 (cited on page 1).

[16] Lucas Koch et al. 'Accurate physics-based modeling of electric vehicle energy consumption in the SUMO traffic microsimulator'. In: *2021 IEEE International Intelligent Transportation Systems Conference (ITSC)*. IEEE. 2021, pp. 1650–1657 (cited on page 1).

[17] Marco Casini, Antonio Vicino, and Giovanni Gino Zanvettor. 'A receding horizon approach to peak power minimization for EV charging stations in the presence of uncertainty'. In: *International Journal of Electrical Power & Energy Systems* 126 (2021), p. 106567 (cited on page 1).

[18] Pengshun Li et al. 'Prediction of electric bus energy consumption with stochastic speed profile generation modelling and data driven method based on real-world big data'. In: *Applied Energy* 298 (2021), p. 117204 (cited on page 1).

[19] Sugam Pokharel, Pradip Sah, and Deepak Ganta. 'Improved prediction of total energy consumption and feature analysis in electric vehicles using machine learning and shapley additive explanations method'. In: *World Electric Vehicle Journal* 12.3 (2021), p. 94 (cited on page 1).

[20] Javier Romero Schmidt and Fernando Auat Cheein. 'Assessment of power consumption of electric machinery in agricultural tasks for enhancing the route planning problem'. In: *Computers and Electronics in Agriculture* 163 (2019), p. 104868 (cited on pages 2, 4, 7).

[21] Cedric De Cauwer, Joeri Van Mierlo, and Thierry Coosemans. 'Energy consumption prediction for electric vehicles based on real-world data'. In: *Energies* 8.8 (2015), pp. 8573–8593 (cited on pages 2, 4, 5, 7).

[22] Sedat Dogru and Lino Marques. 'A physics-based power model for skid-steered wheeled mobile robots'. In: *IEEE Transactions on Robotics* 34.2 (2018), pp. 421–433 (cited on pages 2, 4–6, 16).

[23] T Li et al. 'Real-time adaptive energy management strategy for dual-motor-driven electric tractors'. In: *Trans. Chin. Soc. Agric. Mach* 51 (2020), pp. 530–543 (cited on page 2).

[24] Hamed Farhadi Gharibeh, Ahmad Sadeghi Yazdankhah, and Mohammad Reza Azizian. 'Energy management of fuel cell electric vehicles based on working condition identification of energy storage systems, vehicle driving performance, and dynamic power factor'. In: *Journal of Energy Storage* 31 (2020), p. 101760 (cited on page 2).

[25] Fengqi Zhang et al. 'Energy management strategies for hybrid electric vehicles: Review, classification, comparison, and outlook'. In: *Energies* 13.13 (2020), p. 3352 (cited on page 2).

[26] Xiaodan Xu, HM Abdul Aziz, and Randall Guensler. 'A modal-based approach for estimating electric vehicle energy consumption in transportation networks'. In: *Transportation Research Part D: Transport and Environment* 75 (2019), pp. 249–264 (cited on pages 2, 4).

[27] Ahmad Yulianto et al. 'Modelling of full electric and hybrid electric fuel cells buses'. In: *Procedia computer science* 112 (2017), pp. 1916–1925 (cited on page 2).

[28] Jinghui Wang and Hesham A Rakha. 'Electric train energy consumption modeling'. In: *Applied energy* 193 (2017), pp. 346–355 (cited on page 2).

[29] Dapai Shi et al. 'Energy control strategy of HEB based on the instantaneous optimization algorithm'. In: *IEEE Access* 5 (2017), pp. 19876–19888 (cited on page 4).

[30] Chiara Fiori, Kyoungho Ahn, and Hesham A Rakha. 'Power-based electric vehicle energy consumption model: Model development and validation'. In: *Applied Energy* 168 (2016), pp. 257–268 (cited on pages 4, 6).

[31] Thomas Moore and Daniel Stouch. 'A generalized extended kalman filter implementation for the robot operating system'. In: *Intelligent Autonomous Systems 13: Proceedings of the 13th International Conference IAS-13*. Springer. 2016, pp. 335–348 (cited on page 16).